

Article

Coupling Efficiency of a Partially Coherent Radially Polarized Vortex Beam into a Single-Mode Fiber

Xinlei Zhu ¹ , Kuilong Wang ², Fei Wang ¹, Chengliang Zhao ^{1,*}  and Yangjian Cai ^{1,3}¹ School of Physical Science and Technology, Soochow University, Suzhou 215006, China;

xlzhu@stu.suda.edu.cn (X.Z.); wangfei.phy@163.com (F.W.); yangjiancai@suda.edu.cn (Y.C.)

² Department of Physics, Hangzhou Normal University, Hangzhou 310036, China; wangklzj@126.com³ Center of Light Manipulation and Application, School of Physics and Electronics, Shandong Normal University, Jinan 250014, China

* Correspondence: zhaochengliang@suda.edu.cn; Tel.: +86-151-9008-1996

Received: 27 June 2018; Accepted: 4 August 2018; Published: 7 August 2018



Abstract: We study the problem of coupling partially coherent radially polarized (PCRP) vortex beams into a single-mode optical fiber. Using the well-known concept of the cross-spectral density (CSD) matrix, we derive a general expression for the coupling efficiency of the partially coherent beam into a single-mode fiber. We adopt PCRP vortex beams for incident beams and use our general results to discuss the effects of the coherence, topological charge, and wavelength on the coupling efficiency of an optical beam focused onto a single-mode fiber with a lens. Our results should be useful for any application that requires coupling of partially coherent beams into optical fibers.

Keywords: coupling efficiency; partially coherent; vortex beam; single-mode fiber

1. Introduction

Optical fiber, as the fundamental optical components of a coupling process, have been widely applied in various fields, such as networking [1,2], lidar [3,4], imaging [5], free-space optical communications [6,7], and biomedical optics [8–10]. In the above applications, the input beam must be coupled into a single-mode or multi-modes fiber for propagation and detection before being amplified. Therefore, the coupling efficiency of the input light beam into optical fiber plays an important role. One can improve the signal-to-noise ratio and save energy through increasing the coupled light beam. During the past decades, many theoretical methods and experimental techniques were used to improve the coupling efficiency, such as a fiber array [11], cylindrical glass fiber [12], wedge-shaped fiber endface [13], combination lens [14], chemically etched self-centered diffracting element [15], and a microlens [16].

The degree of freedom of the input light beam, such as phase, amplitude, coherence, and polarization, is one of the key factors when analyzing the coupling efficiency. For example, the coupling efficiency of the plane-wave to fiber was studied as the input light in detail, the influences caused by the misalignments of the fibers and mode's field distribution are considered [17]. Ruilier and Cassaing discussed the coupling efficiency when the stellar is coupled into the single mode fiber [18]. Wheeler and Schmidt developed analytic equations that describe the mean and normalized variance of the coupling efficiency of the Gaussian Schell-model (GSM) beams into single-mode optical fibers [19]. The light sources in the above studies were scalar beams and did not consider the vector beams. In 2009, the polarization state of the beam was first taken into account by Salem and Agrawal. They studied the problem of coupling an electromagnetic beam of any state of coherence and polarization into a multimode optical fiber. The coherence and polarization properties of the electromagnetic Gaussian Schell-model (EGSM) beams are discussed in detail in Refs. [20,21]. In 2012, Zhao and others

demonstrated experimentally the procedure of coupling of an EGSM beam into a single-mode optical fiber. The results showed that the coupling efficiency depends closely on the coherence and polarization properties of the EGSM beam, which is consistent with Salem and Agrawal’s theoretical prediction [22]. Furthermore, in the past several years, due to the partially coherent radially polarized (PCRP) beam having an advantage over a linearly polarized partially coherent beam for reducing turbulence-induced scintillation, which is useful in free-space optical communications, the PCRP beam was introduced in theory and generated in experiment [23–25]. The propagation properties of a PCRP beam are quite different from those of a radially polarized beam. On the other hand, it is well known that any beam with a helical phase factor, called a vortex beam, possesses an optical vortex and carries orbital angular momentum (OAM). Thus, there are growing interests in focusing partially coherent radially polarized vortex beams [26–29]. However, to the best of our knowledge, there are no papers dealing with the coupling efficiency of the PCRP vortex beam into a single-mode fiber.

In this paper, our aim is to study the coupling efficiency of PCRP vortex beams into a single-mode optical fiber. Analytical expressions for the coupling efficiency are derived based on the concept of the cross-spectral density matrix. The effects caused by the coherence, topological charge, numerical aperture (NA), and wavelength on the coupling efficiency are studied in detail. We calculate the peak coupling efficiency versus the NA for different coherence length and topological charge. One can choose suitable spatial coherence and topological charge to obtain optimal results for different applications. We believe that it has important applications in free-space optical communication.

2. Coupling Efficiency of Partially Coherent Radially Polarized Vortex Beams

The schematic diagram of our coupling arrangement is shown in Figure 1. Suppose that a PCRP vortex beam is coupled into a single-mode fiber by a lens of focal length f . Let the coordinate in the plane A be denoted by ρ . Based on the theory of coherence and polarization, the second-order statistical properties of a PCRP beam can be characterized by the 2×2 CSD matrix $\overset{\leftrightarrow}{W}(\rho_1, \theta_1, \rho_2, \theta_2)$ in the plane A, which are defined as [22,23]:

$$\begin{aligned} W_{0xx}(\rho_1, \theta_1, \rho_2, \theta_2) &= \frac{\rho_1 \rho_2 \cos \theta_1 \cos \theta_2}{4w_0^2} \exp\left(-\frac{\rho_1^2 + \rho_2^2}{4w_0^2}\right) \exp\left[-\frac{\rho_1^2 + \rho_2^2 - 2\rho_1 \rho_2 \cos(\theta_1 - \theta_2)}{2\delta_0^2}\right] \\ W_{0xy}(\rho_1, \theta_1, \rho_2, \theta_2) &= \frac{\rho_1 \rho_2 \cos \theta_1 \sin \theta_2}{4w_0^2} \exp\left(-\frac{\rho_1^2 + \rho_2^2}{4w_0^2}\right) \exp\left[-\frac{\rho_1^2 + \rho_2^2 - 2\rho_1 \rho_2 \cos(\theta_1 - \theta_2)}{2\delta_0^2}\right] \\ W_{0yx}(\rho_1, \theta_1, \rho_2, \theta_2) &= W_{0xy}^*(\rho_1, \theta_1, \rho_2, \theta_2) \\ W_{0yy}(\rho_1, \theta_1, \rho_2, \theta_2) &= \frac{\rho_1 \rho_2 \sin \theta_1 \sin \theta_2}{4w_0^2} \exp\left(-\frac{\rho_1^2 + \rho_2^2}{4w_0^2}\right) \exp\left[-\frac{\rho_1^2 + \rho_2^2 - 2\rho_1 \rho_2 \cos(\theta_1 - \theta_2)}{2\delta_0^2}\right] \end{aligned} \tag{1}$$

where w_0 is the beam width in the plane A and δ_0 is the spatial coherence length. PCRP beams can be embedded a vortex phase, and the new CSD of PCRP vortex beams can be rewritten as follows [28]

$$W_{\alpha\beta}(\rho_1, \theta_1, \rho_2, \theta_2) = W_{0\alpha\beta}(\rho_1, \theta_1, \rho_2, \theta_2) \exp(-im\theta_1 + im\theta_2) \tag{2}$$

where m is the topological charge. According to the coupling theory introduced in Ref. [28], the field distribution of the fiber mode can be approximated by a Gaussian function [30,31]:

$$F_j = \sqrt{\frac{2}{\pi}} \omega_j^{-1} \exp\left(-\frac{\rho_j^2}{\omega_j^2}\right) \quad (j = x, y) \tag{3}$$

where ρ' is a transverse position vector in the fiber plane B and ω_j is a measure of the mode width. Furthermore, the field distribution of the mode at the aperture plane A is found by using the backpropagation technique from B to A and is given by:

$$F_{jA} = \sqrt{\frac{2}{\pi}} \omega_{jA}^{-1} \exp\left(-\frac{\rho^2}{\omega_{jA}^2}\right) \tag{4}$$

where $\omega_{jA} = \lambda f / \pi \omega_j$ is the effective mode width at the aperture plane, λ is the wavelength of the incident, and f is the focal length of the coupling lens. We can get the coupling efficiency as:

$$\eta_c = \frac{\langle P_c \rangle}{\langle P_a \rangle} \tag{5}$$

where $\langle P_c \rangle$ is the power coupled into the fiber and $\langle P_a \rangle$ is the power in the aperture plane. They can be expressed as:

$$\begin{aligned} P_c &= \iint_D W_{ij}(\rho_1, \rho_2, \omega) F_{iA}^*(\rho_1) F_{jA}(\rho_2) \times \exp\left(-\frac{\rho_1^2 + \rho_2^2}{W^2}\right) d^2 \rho_1 d^2 \rho_2 \\ P_a &= \int_D W_{jj}(\rho, \rho, \omega) \times \exp\left(-\frac{2\rho^2}{W^2}\right) d^2 \rho \end{aligned} \quad (j = x, y) \tag{6}$$

where D denotes a hard aperture of diameter, $W^2 = D^2/8$, and $NA = D/2f$ [32].

For PCRP vortex beams, we obtain the following expression for the power coupled into the single fiber with P_{c_even} (m is even number) and P_{c_odd} (m is odd number):

$$\begin{aligned} P_{c_even} &= \frac{\pi}{2\omega_0^2 \omega_{xA}^2} \left[\sum_{s=0}^{\infty} \frac{1}{s! \Gamma(|m-1|+s+1)} \left(\frac{1}{2\delta_0^2}\right)^{|m-1|+2s} \frac{1}{A_x^{|m-1|+2s+3}} \left(\frac{|m-1|+2s+1}{2}\right)! \left(\frac{|m-1|+2s+1}{2}\right)! \right. \\ &\quad \left. + \sum_{s=0}^{\infty} \frac{1}{s! \Gamma(|m+1|+s+1)} \left(\frac{1}{2\delta_0^2}\right)^{|m+1|+2s} \frac{1}{A_x^{|m+1|+2s+3}} \left(\frac{|m+1|+2s+1}{2}\right)! \left(\frac{|m+1|+2s+1}{2}\right)! \right] \\ &\quad + \frac{\pi}{2\omega_0^2 \omega_{yA}^2} \left[\sum_{s=0}^{\infty} \frac{1}{s! \Gamma(|m-1|+s+1)} \left(\frac{1}{2\delta_0^2}\right)^{|m-1|+2s} \frac{1}{A_y^{|m-1|+2s+3}} \left(\frac{|m-1|+2s+1}{2}\right)! \left(\frac{|m-1|+2s+1}{2}\right)! \right. \\ &\quad \left. + \sum_{s=0}^{\infty} \frac{1}{s! \Gamma(|m+1|+s+1)} \left(\frac{1}{2\delta_0^2}\right)^{|m+1|+2s} \frac{1}{A_y^{|m+1|+2s+3}} \left(\frac{|m+1|+2s+1}{2}\right)! \left(\frac{|m+1|+2s+1}{2}\right)! \right] \end{aligned} \tag{7}$$

$$\begin{aligned} P_{c_odd} &= \frac{\pi^2}{2A_x \omega_0^2 \omega_{xA}^2} \left[\sum_{s=0}^{\infty} \frac{1}{s! \Gamma(|m-1|+s+1)} \left(\frac{1}{2\delta_0^2}\right)^{|m-1|+2s} \frac{1}{(2A_x)^{|m-1|+2s+2}} (|m-1|+2s+1)!! (|m-1|+2s+1)!! \right. \\ &\quad \left. + \sum_{s=0}^{\infty} \frac{1}{s! \Gamma(|m+1|+s+1)} \left(\frac{1}{2\delta_0^2}\right)^{|m+1|+2s} \frac{1}{(2A_x)^{|m+1|+2s+2}} (|m+1|+2s+1)!! (|m+1|+2s+1)!! \right] \\ &\quad + \frac{\pi^2}{2A_y \omega_0^2 \omega_{yA}^2} \left[\sum_{s=0}^{\infty} \frac{1}{s! \Gamma(|m-1|+s+1)} \left(\frac{1}{2\delta_0^2}\right)^{|m-1|+2s} \frac{1}{(2A_y)^{|m-1|+2s+2}} (|m-1|+2s+1)!! (|m-1|+2s+1)!! \right. \\ &\quad \left. + \sum_{s=0}^{\infty} \frac{1}{s! \Gamma(|m+1|+s+1)} \left(\frac{1}{2\delta_0^2}\right)^{|m+1|+2s} \frac{1}{(2A_y)^{|m+1|+2s+2}} (|m+1|+2s+1)!! (|m+1|+2s+1)!! \right] \end{aligned} \tag{8}$$

where $A_x = 1/\omega_0^2 + 1/(2\delta_0^2) + 1/\omega_{xA}^2 + 1/D^2$, and $A_y = 1/\omega_0^2 + 1/(2\delta_0^2) + 1/\omega_{yA}^2 + 1/D^2$.

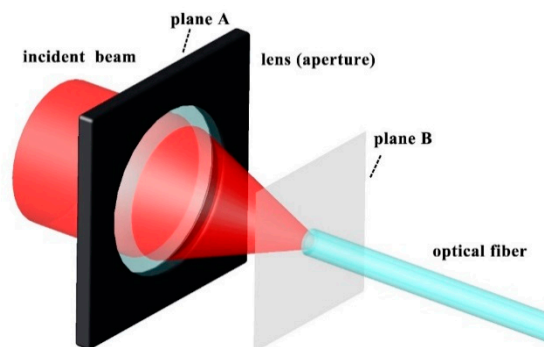


Figure 1. Illustrating notation related to the coupling of a beam into an optical fiber.

The power of the input PCRP vortex beams at the aperture plane is

$$P_a = \frac{\pi}{4\omega_0^2} \left(\frac{1}{\omega_0^2} + \frac{1}{W^2} \right)^{-2} \tag{9}$$

3. Results and Discussion

In this section, with the help of the formulas obtained in Section 2, we will study the coupling efficiency of PCRP vortex beams for different topological charges, coherence length, and wavelength. First, we carefully chose the values of $\omega_j (j = x, y)$ in Equation (3) to match with the core radius of the fiber because the theoretical model is only valid for the single-mode fiber. Let us recall the definition of the normalized frequency of the fiber [33]

$$V = \frac{2\pi a}{\lambda} \sqrt{n_1^2 - n_2^2} \tag{10}$$

where a is the radius of the fiber core, λ is the wavelength of the incident light. n_1 and n_2 are the peak values of the refractive index of the fiber core and the refractive index of the fiber cladding, respectively. It is known that when the value of V is smaller than 2.405, the fiber belongs to the single-mode fiber. Assuming that the fiber is weakly guiding with the refractive index profile, the last term in Equation (9) can be written as $\sqrt{n_1^2 - n_2^2} \approx n_1 \sqrt{2\Delta}$ with $\Delta = (n_1 - n_2)/n_1$ as a good approximation. To ensure the single-mode fiber, the parameter is chosen to be $a = 5 \mu\text{m}$, $n_1 = 1.44$, $\Delta = 0.0034$, and $\lambda = 1550 \text{ nm}$. On substituting these parameters into Equation (9), we obtained a value of V of 2.4, smaller than 2.405. Under this condition, we found the radius of the mode field of the fundamental propagating mode in the fiber by using the empirical formula to be $\omega_j = 5.15 \mu\text{m} (j = x, y)$. Therefore, in the following numerical examples, the value of ω_j was kept fixed at $5.15 \mu\text{m}$ throughout the paper. If the focal length of the lens in plane A is 10 cm, the radius $\omega_{jA} (j = x, y)$ of the mode field was calculated to be 9.6 mm.

Figure 2 shows the intensity distribution of PCRP vortex beams in plane B with different spatial coherence width and topological charge. The propagation properties of PCRP vortex beams through a paraxial ABCD optical system have been studied in Ref. [28]. Figure 2 shows that the focusing properties of a PCRP vortex beam are closely affected by its initial spatial coherence and topological charge. The beam spot got larger with increasing topological charge from $m = 1$ to 3, but not $m = 0$. This is because the PCRP vortex beam became the PCRP beam for $m = 0$, which has a ring-shaped beam profile. The PCRP vortex beam had a dark hollow beam spot (see Figure 2h) with large coherence. When the spatial coherence was decreased, a flat-topped beam spot was formed (see Figure 2d). With the further decrease of the spatial coherence, a focused Gaussian beam spot was formed.

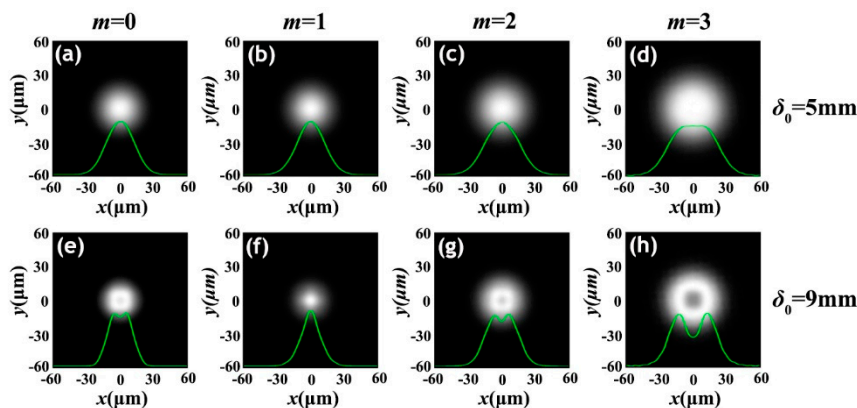


Figure 2. Distribution of the intensity of PCRP vortex beams in plane B for different coherence length and topological charge.

Figure 3 shows that the coupling efficiency varied with NA for different values of δ_0 under different topological charges. In Figure 3, one can find that the coupling efficiency increased at first and then decreased with increasing NA, and there was a peak value of the coupling efficiency, which means there was a best match between the incident beam and the distribution of the mode field. We also confirm that the position of the peak (i.e., the value of NA) was different for different coherence length and topological charge. We could adjust the spatial coherence to improve the coupling efficiency, and an optimum value was found. Obviously, the result of Figure 3b is different to other results. We found that when PCRP vortex beams had $m = 1$, the coupling efficiency increased with the increasing of the spatial coherence width of the beam. We can explain this phenomenon using the property of PCRP vortex beams (see Figure 2), where the PCRP vortex beams with $m = 1$ have a similar Gauss distribution beam profile.

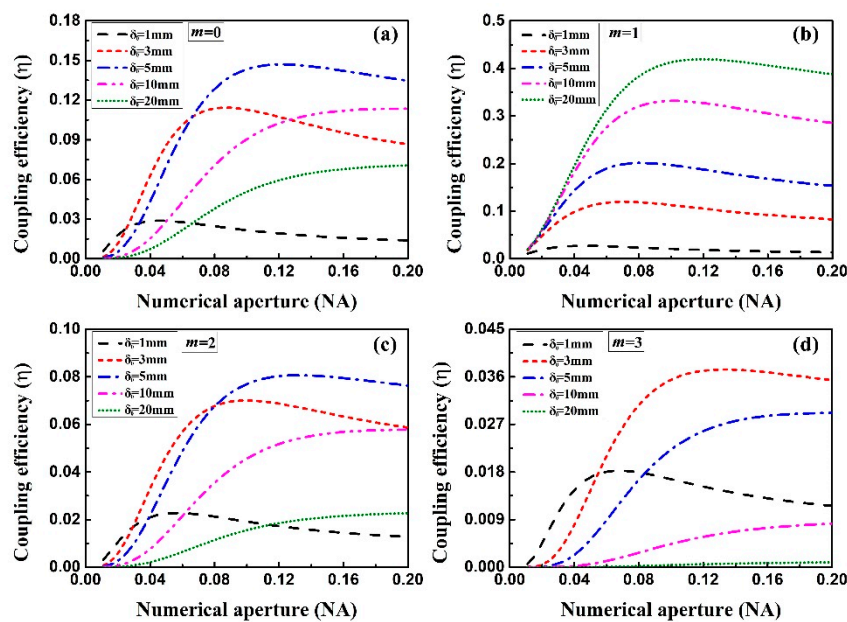


Figure 3. The coupling efficiency of the symmetric beam with $\omega_0 = 10$ mm and $\lambda = 1550$ nm varied with NA for different values of δ_0 under different topological charges.

Based the analysis above, we know that there is a best choice (peak value of the coupling efficiency) of the value of coherence and NA for different topological charge. Next, we simulated how the density plot of the coupling efficiency varied with NA and initial spatial coherence under different topological charges in Figure 4. In Figure 4, the numbers in brackets are the peak value of the coupling efficiency and corresponding value of the NA and spatial coherence width. One can clearly see the distribution of the coupling efficiency in the whole region under different topological charges. One can also find out clearly the peak of the coupling efficiency under different topological charges and the corresponding value of the coherence length and NA. Therefore, for the suitable value of δ_0 and m , we could obtain the maximum coupling efficiency.

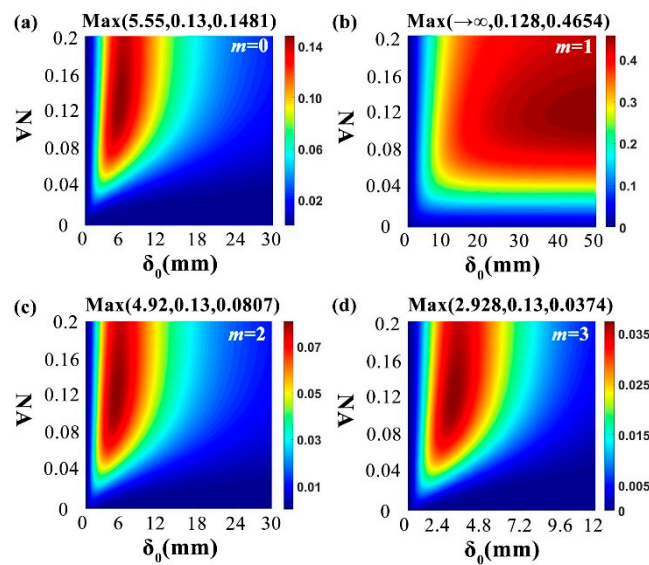


Figure 4. The density plot distribution of how the coupling efficiency of the symmetric beam with $\omega_0 = 10$ mm and $\lambda = 1550$ nm varies with numerical aperture and initial spatial coherence under different topological charges.

Figure 5 shows the coupling efficiency of the beam versus NA for different wavelengths λ under different topological charges. From Figure 5, we can find that all the coupling efficiencies showed the similar change rule for smaller topological charges (see Figure 5a–c); the coupling efficiency increased at first and then decreased with increasing NA, and there was a peak value of the coupling efficiency. However, the coupling efficiency increased with decreasing wavelength for smaller NA (for example, $NA < 0.08$), and for larger NA (for example, $NA > 0.16$), the coupling efficiency increased with the increasing wavelength. However, for larger topological charges (for example $m > 3$, we did not plot it in here), we found that the coupling efficiency shows the same change rule as Figure 5d; it increases with the increasing of NA and wavelength. Moreover, from Figure 5b, we could also find that the coupling efficiency showed some different change rule due to the different properties of PCRP vortex beams with $m = 1$.

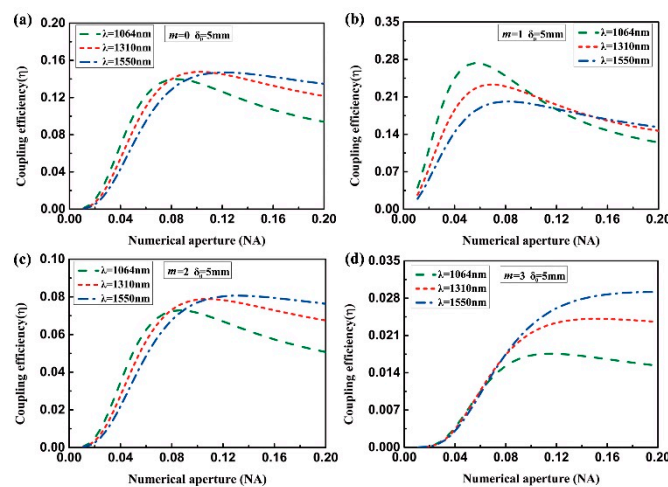


Figure 5. The coupling efficiency of the beam with $\delta_0 = 5$ mm, $\omega_0 = 10$ mm versus numerical aperture for different wavelengths λ under different topological charges.

4. Conclusions

In this paper, we derived a general expression for the coupling efficiency of PCRVP vortex beams into a single-mode optical fiber in terms of its CSD matrix. We were able to derive an analytical expression for the coupling efficiency, and the field distribution of the fundamental mode of an optical fiber is approximated. We studied the effects of the coherence, topological charge and wavelength of the PCRVP vortex beams, and NA on the coupling efficiency through some numerical simulation. The results showed that the coupling efficiency was significantly affected by the numerical aperture and parameters of the incident beam, such as topological charge, initial spatial coherence, and wavelength, and we also determined the best choice for the PCRVP vortex beams with different topological charge. Our results will help users to determine for themselves which initial beam parameters and NA provides optimal results for their applications. It should be useful for any application requiring coupling of a partially coherent radially polarized vortex beam into optical fibers.

Author Contributions: X.Z. (Data curation, Writing-original draft, Methodology); K.W. (Formal analysis, Writing-review and editing); F.W. (Supervision, Writing-review and editing); C.Z. (Supervision, Project administration, Writing-review and editing), Y.C. (Supervision, Project administration, Writing-review and editing).

Funding: This research was funded by the National Natural Science Foundation of China [grant number 11774250 and 91750201]; National Natural Science Fund for Distinguished Young Scholar [grant number 11525418].

Conflicts of Interest: The authors declare no conflict of interest.

References

1. Cantono, M.; Ferrari, A.; Waheed, U.; Ahmad, A.; Zaidi, S.H.; Bianco, A.; Curri, V. Networking benefit of hybrid fiber amplification for lightpath regenerators saving. In Proceedings of the Optical Fiber Communication Conference, Los Angeles, CA, USA, 19–23 March 2017; Optical Society of America: Washington, DC, USA, 2017.
2. Prucnal, P.; Santoro, M.; Fan, T. Spread spectrum fiber-optic local area network using optical processing. *J. Lightw. Technol.* **1986**, *4*, 547–554. [[CrossRef](#)]
3. Yun, J.; Gao, C.; Zhu, S.; Sun, C.; He, H.; Feng, L.; Dong, L.; Niu, L. High-peak-power, single-mode, nanosecond pulsed, all-fiber laser for high resolution 3D imaging LIDAR system. *Chin. Opt. Lett.* **2012**, *10*, 121402.
4. Li, S.; Hua, D.; Wang, L.; Song, Y. Analysis of an efficient single-mode fiber coupler for all-fiber rotational Raman lidar. *Optik* **2013**, *124*, 1450–1454. [[CrossRef](#)]
5. Choi, Y.; Yoon, C.; Kim, M.; Yang, T.D.; Fang-Yen, C.; Dasari, R.R.; Lee, K.J.; Choi, W. Scanner-free and wide-field endoscopic imaging by using a single multimode optical fiber. *Phys. Rev. Lett.* **2012**, *109*, 203901. [[CrossRef](#)] [[PubMed](#)]
6. Ma, J.; Zhao, F.; Tan, L.; Yu, S.; Yang, Y. Degradation of single-mode fiber coupling efficiency due to localized wavefront aberrations in free-space laser communications. *Opt. Eng.* **2010**, *49*, 045004. [[CrossRef](#)]
7. Bozinovic, N.; Yue, Y.; Ren, Y.; Tur, M.; Kristensen, P.; Huang, H.; Willner, A.E.; Ramachandran, S. Terabit-Scale Orbital Angular Momentum Mode Division Multiplexing in Fibers. *Science* **2013**, *340*, 1545–1548. [[CrossRef](#)] [[PubMed](#)]
8. Papadopoulos, I.N.; Farahi, S.; Moser, C.; Psaltis, D. High-resolution, lensless endoscope based on digital scanning through a multimode optical fiber. *Biomed. Opt. Express* **2013**, *4*, 260–270. [[CrossRef](#)] [[PubMed](#)]
9. Eugui, P.; Lichtenegger, A.; Augustin, M.; Harper, D.J.; Fialová, S.; Wartak, A.; Hitzberger, C.K.; Baumann, B. Few-mode fiber detection for tissue characterization in optical coherence tomography. In Proceedings of the European Conferences on Biomedical Optics, International Society for Optics and Photonics, Munich, Germany, 25–29 June 2017; p. 104160M.
10. Woyessa, G.; Fasano, A.; Stefani, A.; Markos, C.; Nielsen, K.; Rasmussen, H.K.; Bang, O. Single mode step-index polymer optical fiber for humidity insensitive high temperature fiber Bragg grating sensors. *Opt. Express* **2016**, *24*, 1253–1260. [[CrossRef](#)] [[PubMed](#)]
11. Hahn, D.V.; Brown, D.M.; Rolander, N.W.; Sluz, J.E.; Venkat, R. Fiber optic bundle array wide field-of-view optical receiver for free space optical communications. *Opt. Lett.* **2010**, *35*, 3559–3561. [[CrossRef](#)] [[PubMed](#)]

12. Weidel, E. New coupling method for GaAs-laser–fibre coupling. *Electron. Lett.* **1975**, *11*, 436–437. [[CrossRef](#)]
13. Shah, V.S.; Curtis, L.; Vodhanel, R.S.; Bour, D.P.; Young, W.C. Efficient power coupling from a 980-nm, broad-area laser to a single-mode fiber using a wedge-shaped fiber endface. *J. Lightw. Technol.* **1990**, *8*, 1313–1318. [[CrossRef](#)]
14. Kawano, K.; Mitomi, O.; Saruwatari, M. Combination lens method for coupling a laser diode to a single-mode fiber. *Appl. Opt.* **1985**, *24*, 984–989. [[CrossRef](#)] [[PubMed](#)]
15. Kayoun, P.; Puech, C.; Papuchon, M.; Arditty, H. Improved coupling between laser diode and single-mode fibre tipped with a chemically etched self-centred diffracting element. *Electron. Lett.* **1981**, *17*, 400–402. [[CrossRef](#)]
16. Kotsas, A.; Ghafouri-Shiraz, H.; Maclean, T. Microlens fabrication on single-mode fibres for efficient coupling from laser diodes. *Opt. Quant. Electron.* **1991**, *23*, 367–378. [[CrossRef](#)]
17. Lazzaroni, M.; Zocchi, F.E. Optical coupling from plane wave to step-index single-mode fiber. *Opt. Commun.* **2004**, *237*, 37–43. [[CrossRef](#)]
18. Ruilier, C.; Cassaing, F. Coupling of large telescopes and single-mode waveguides: Application to stellar interferometry. *J. Opt. Soc. Am. A* **2001**, *18*, 143–149. [[CrossRef](#)]
19. Wheeler, D.J.; Schmidt, J.D. Coupling of Gaussian Schell-model beams into single-mode optical fibers. *J. Opt. Soc. Am. A* **2011**, *28*, 1224–1238. [[CrossRef](#)] [[PubMed](#)]
20. Salem, M.; Agrawal, G.P. Effects of coherence and polarization on the coupling of stochastic electromagnetic beams into optical fibers. *J. Opt. Soc. Am. A* **2009**, *26*, 2452–2458. [[CrossRef](#)] [[PubMed](#)]
21. Salem, M.; Agrawal, G.P. Coupling of stochastic electromagnetic beams into optical fibers. *Opt. Lett.* **2009**, *34*, 2829–2831. [[CrossRef](#)] [[PubMed](#)]
22. Zhao, C.; Dong, Y.; Wu, G.; Wang, F.; Cai, Y.; Korotkova, O. Experimental demonstration of coupling of an electromagnetic Gaussian Schell-model beam into a single-mode optical fiber. *Appl. Phys. B* **2012**, *108*, 891–895. [[CrossRef](#)]
23. Wu, G.; Wang, F.; Cai, Y. Coherence and polarization properties of a radially polarized beam with variable spatial coherence. *Opt. Express* **2012**, *20*, 28301–28318. [[CrossRef](#)] [[PubMed](#)]
24. Wang, F.; Cai, Y.; Dong, Y.; Korotkova, O. Experimental generation of a radially polarized beam with controllable spatial coherence. *Appl. Phys. Lett.* **2012**, *100*, 051108. [[CrossRef](#)]
25. Zhu, S.; Zhu, X.; Liu, L.; Wang, F.; Cai, Y. Theoretical and experimental studies of the spectral changes of a polychromatic partially coherent radially polarized beam. *Opt. Express* **2013**, *21*, 27682–27696. [[CrossRef](#)] [[PubMed](#)]
26. Chen, Z.; Cui, S.; Zhang, L.; Sun, C.; Xiong, M.; Pu, J. Measuring the intensity fluctuation of partially coherent radially polarized beams in atmospheric turbulence. *Opt. Express* **2014**, *22*, 18278–18283. [[CrossRef](#)] [[PubMed](#)]
27. Zhu, X.; Wu, G.; Liu, L.; Zhu, S.; Cai, Y. Statistical properties of a partially coherent radially polarized beam propagating through an astigmatic optical system. *Opt. Commun.* **2014**, *316*, 132–139. [[CrossRef](#)]
28. Guo, L.; Chen, Y.; Liu, X.; Liu, L.; Cai, Y. Vortex phase-induced changes of the statistical properties of a partially coherent radially polarized beam. *Opt. Express* **2016**, *24*, 13714–13728. [[CrossRef](#)] [[PubMed](#)]
29. Zhang, Y.; Zhao, Z.; Ding, C.; Pan, L. Correlation singularities of a partially coherent radially polarized beam in non-Kolmogorov turbulence. *J. Opt.* **2016**, *19*, 025603. [[CrossRef](#)]
30. Marcuse, D. *Theory of Dielectric Optical Waveguides*; Elsevier: New York, NY, USA, 2013.
31. Buck, J.A. *Fundamentals of Optical Fibers*; John Wiley & Sons: Hoboken, NJ, USA, 2004.
32. Andrews, L.C.; Phillips, R.L.; Hopen, C.Y. *Laser Beam Scintillation with Applications*; SPIE Press: Washington, DC, USA, 2001.
33. Marcuse, D. Gaussian approximation of the fundamental modes of graded-index fibers. *J. Opt. Soc. Am. A* **1978**, *68*, 103–109. [[CrossRef](#)]

